ACADEMIC PRESS

Available online at www.sciencedirect.com
SCIENCE DIRECT®

Journal of Catalysis 217 (2003) 468–477

JOURNAL OF CATALYSIS

www.elsevier.com/locate/jcat

Tantalum oxide-supported metal oxide (Re_2O_7, CrO_3, MoO_3, WO_3, V_2O_5, and Nb_2O_5) catalysts: synthesis, Raman characterization and chemically probed by methanol oxidation

Yongsheng Chen and Israel E. Wachs *

In Situ Molecular Characterization & Catalysis Laboratory, Department of Chemical Engineering, Lehigh University, Bethlehem, PA 18015, USA

Received 9 December 2002; revised 3 February 2003; accepted 10 February 2003

Abstract

The molecular structures and reactivity of tantalum oxide-supported metal oxide (V_2O_5, Nb_2O_5, CrO_3, MoO_3, WO_3, and Re_2O_7) catalysts were determined by Raman spectroscopy and the methanol oxidation chemical probe reaction, respectively. The metal oxides form a two-dimensional surface metal oxide overlayer on the tantalum oxide support. Under ambient conditions, the hydrated surface metal oxide species possesses structures similar to the corresponding metal oxide ionic species present in acidic solutions (ReO_4^-, $Cr_2O_7^{2-}$, $Mo_8O_{26}^{4-}$, $HW_{12}O_{42}^{10-}$, $V_{10}O_{28}^{6-}$, and $Nb_2O_5 \cdot nH_2O$). Under dehydrated conditions, only one surface ReO_x species is present on the tantalum oxide support. For CrO_3, MoO_3, WO_3, V_2O_5, and Nb_2O_5 supported on tantalum oxide, two dehydrated surface metal oxide species may be present: isolated and/or polymerized species. During methanol oxidation, the surface vanadium, chromium, and rhenium oxide sites on the tantalum oxide support behave as surface redox sites, while the surface tungsten and niobium oxide sites on the tantalum oxide support are surface acidic sites. The surface molybdenum oxide sites on tantalum oxide possess both acidic and redox characteristics. No surface basic sites were found on any of the tantalum oxide-supported metal oxide catalysts. The relative redox activity and selectivity of the various tantalum oxide-supported metal oxides reflect the catalytic properties of the pure metal oxides.

Keywords: Catalysts; Metal oxides; Supported; Raman spectroscopy; BET; Oxidation; Methanol; Selectivity; Activity; TOF

1. Introduction

Supported metal oxide catalysts have numerous applications in the petroleum, chemical, and pollution control industries [1,2]. By depositing active metal oxides (Re_2O_7, CrO_3, MoO_3, WO_3, V_2O_5, Nb_2O_5, etc.) on high surface area oxide supports (Al_2O_3, SiO_2, TiO_2, ZrO_2, etc.), the dispersion and catalytic efficiency of the active metal oxide components can be significantly altered. Below monolayer surface coverage, where only the surface MO_x species is present on the oxide supports, an opportunity exists for varying the catalytic properties through a judicious selection of the specific oxide support. The support effect can markedly alter the turnover frequency (TOF: number of specific reaction molecules generated per active surface site per second) over many orders of magnitude [3] and even affect the acidic and redox characteristics of the surface MO_x species [4]. Supported chromium oxide catalysts are active for catalytic destruction of perchloroethylene [5], dehydrogenation of ethane with carbon dioxide [6,7], and olefin polymerization [8]. Supported molybdenum oxide catalysts find applications in selective oxidation of methanol and ethanol [9,10], direct conversion of methane to aromatics [11–13], and hydrodesulfurization (HDS)/hydrodenitrogenation (HDN) of petroleum feedstocks [14]. Supported tungsten oxide catalysts have been investigated for alkane isomerization [15,16] and hydrocarbon conversion cracking catalysts [17] and are also employed as HDS/HDN catalysts in the petroleum industry [1]. Supported rhenium oxide catalysts are employed as olefin metathesis catalysts [18] and have been investigated for selective oxidation of methanol to methylal [19] and formaldehyde [20]. Supported group 5 metal oxides (V_2O_5 and Nb_2O_5) have a variety of applications, which have been extensively investigated [21–24]. Supported vanadium oxide catalysts possess outstanding redox properties and are primarily employed as selective oxidation catalysts. Supported

* Corresponding author.
E-mail address: iew0@lehigh.edu (I.E. Wachs).

0021-9517/03/$ – see front matter
doi:10.1016/S0021-9517(03)00065-4

niobium oxide catalysts usually possess acidic properties, and reactions requiring acidity are usually investigated with these catalysts. Interestingly, Nb_2O_5/SiO_2 is unique in that it exhibits redox properties during conventional oxidation reactions as well as photocatalytic oxidation reactions. However, no studies have been reported for any of these supported metal oxides on a tantalum oxide support.

Heterogeneous catalytic reactions occur on the surface of catalysts and, hence, the molecular structures of the active surface metal oxide species are very important to determine in order to better understand the catalytic properties. Efforts have been made to clarify the molecular structures of the surface metal oxide species present in supported metal oxides and build relationships with their catalytic properties in order to design and/or improve such catalysts for specific applications [25,26]. Many physical techniques have been employed in these studies, such as Raman, IR, EXAFS, XANES, solid-state NMR, UV–Vis–NIR DRS, and XPS. Raman and IR spectroscopies are able to detect the characteristic vibrations of specific functional groups of the surface metal oxide species and, thus, provide direct insight into their molecular structures. Wachs and co-workers have systematically employed Raman and IR to characterize the supported metal oxides and clarified their molecular structures [27]. The molecular structures were found to be governed under different rules for hydrated and dehydrated conditions. Under hydrated conditions, the surfaces of the catalysts are covered by a thin film of water and the aqueous solution chemistry determines the hydrated molecular structures. For hydrated supported metal oxides, the oxide support and the surface metal oxide concentration in the aqueous film determine the aqueous equilibrium pH at PZC (point of zero charge), which determines the hydrated metal oxide molecular structures [27]. Under acidic aqueous solutions, the supported metal oxides take the following forms: $Cr_3O_{10}^{2-}$ [28], $Mo_8O_{26}^{4-}$ [29], $Nb_2O_5 \cdot nH_2O$ [30], ReO_4^- [31,32], $V_{10}O_{28}^{6-}$ [31], and $W_{12}O_{42}^{12-}$ [33]; while under basic aqueous solutions, the corresponding species are CrO_4^{2-}, MoO_4^{2-}, $Nb_6O_{19}^{8-}$, ReO_4^-, VO_4^{3-}, and WO_4^{2-} [34]. Under dehydrated conditions, the hydrated surface metal oxide clusters decompose and react with the surface hydroxyls of the oxide support. This results in the anchoring of the surface metal oxides to the oxide support via bridging M–O–support bonds (M = the different active surface metal oxides). The dehydrated surface metal oxides possess similar MO_4 coordination at low surface coverage and either MO_4 and/or MO_5/MO_6 structures at monolayer surface coverage, which depends on the specific metal oxide [35–40].

Bulk tantalum oxide is a solid acid catalyst and several applications of supported tantalum oxide catalysts have been reported in recent years [41–45], but there are no fundamental results about tantalum oxide catalysts where it is present as a support for active surface metal oxides. In this paper, tantalum oxide-supported metal oxide catalysts (CrO_3, MoO_3, Nb_2O_5, Re_2O_7, V_2O_5, and WO_3) were prepared via the incipient wetness impregnation method of their precursors and physically characterized with Raman spectroscopy under both hydrated and dehydrated conditions, which allowed determination of the molecular structures of the surface metal oxide species. The catalytic properties of the surface metal oxide species were chemically probed with the methanol oxidation reaction and the relationships between the molecular structure and the catalytic activity/selectivity were investigated.

2. Experimental

2.1. Catalyst preparation

The tantalum oxide support ($S_{BET} = 23\ m^2/g$) was prepared from tantalum oxyhydrate (H.C. Starck, 99.9%) by heat treatment at 600 °C for 12 h. The supported metal oxide (V_2O_5, Nb_2O_5, CrO_3, MoO_3, WO_3, and Re_2O_7) catalysts were prepared by the incipient wetness impregnation method. The support was impregnated with aqueous solutions of the corresponding precursors, which included chromium (III) nitrate ($Cr(NO_3)_3 \cdot 9H_2O$, Alfa Aesar), ammonium heptamolybdate ($(NH_4)_6Mo_7O_{24} \cdot 4H_2O$, Alfa Aesar), niobium oxalate ($Nb(HC_2O_4)_5$, Niobium Products Company), perrhenic acid ($HReO_4$, Alfa Aesar), ammonium vanadium oxide (NH_4VO_3, Alfa Aesar) (oxalic acid added to improve the solubility), and ammonium metatungstate ($(NH_4)_6H_2W_{12}O_{40}$, Pfaltz & Bauer, Inc.). After impregnation, the samples were initially dried at room temperature for about 8 h, subsequently dried at 110 °C for 8 h and then calcined for 8 h at 450 °C for MoO_3/Ta_2O_5 and V_2O_5/Ta_2O_5, and at 500 °C for the other catalysts.

2.2. BET surface area measurement

The BET surface areas of tantalum oxide-supported metal oxide catalysts were obtained with a Quantsorb surface area analyzer (Quantachrome Corporation, Model OS-9) using 3/7 ratio of N_2/He mixture as the exposed gas. Typically, 0.5–1 g of the catalysts was used for the measurement. The catalysts were outgassed at 250 °C prior to the nitrogen physical adsorption at −196 °C, which allowed determination of the BET surface areas.

2.3. Raman spectroscopy

Raman spectra were obtained with the 514.5 nm line of an Ar^+ ion laser (Spectra Physics, Model 164). The exciting laser power was measured at the sample to be about 10–25 mW. The scattered radiation from the sample passed through a SPEX Triplemate monochromator (Model 1877) and was detected by an OMA III (Princeton Applied Research, Model 1463) optical multichannel analyzer with a photodiode array cooled thermoelectrically to −35 °C. The samples were pressed into self-supporting wafers. The

hydrated samples were rotated at 2000 rpm to minimize local heating. The Raman spectra of the dehydrated samples were recorded at room temperature and were obtained after heating the sample in flowing O_2 at 350–450 °C for 1 h in a stationary quartz cell [32].

2.4. Methanol oxidation

The methanol oxidation reaction was carried out in a fixed-bed differential reactor operating at atmospheric pressure. A mixture of helium and oxygen from two mass flow controllers (Brooks 5850) was bubbled through a methanol saturator cooled by flowing water (Neslab RTE 110) to obtain a 6/13/81 mol% mixture of methanol/oxygen/helium at a flow rate of ∼ 100 standard cubic centimeters per minute (sccm). The reactor was vertically held and made of a 6-mm o.d. Pyrex glass and the flow direction was downward. The catalysts were placed at the middle of the tube between two layers of quartz wool. The reaction was carried out at 230 °C and about 100 mg of catalyst was used. Before the methanol oxidation reaction, the catalysts were pretreated at 400 °C for 30 min with flowing oxygen and helium. The outlet of the reactor was maintained at ∼ 120–140 °C in order to avoid condensation of the reaction products. The reaction products were analyzed by an online GC (HP 5840) equipped with TCD and FID detectors, and two GC columns (Carboxene-1000 packed column and CP-sil 5CB capillary column) connected in parallel. The packed column and TCD detector were used to detect CO_x, methanol, and formaldehyde (HCHO), while the capillary column and the FID detector were used for detection of dimethyl ether (DME), methanol, methyl formate (MF), and dimethoxymethane (DMM). The total conversion of methanol was maintained below 10% in order to obtain differential kinetic data and minimize heat and mass transfer limitations. The selectivities, activities, and TOF values were determined for each of the catalysts. The TOF values were calculated by normalizing the reaction rates to the number of surface metal oxide species since they were 100% dispersed below monolayer surface coverage.

3. Results

3.1. Raman spectroscopy

3.1.1. Determination of monolayer surface coverage of Ta_2O_5-supported metal oxides

The Raman spectra of the hydrated tantalum oxide-supported metal oxide systems are presented in Figs. 1–6: Re_2O_7/Ta_2O_5, CrO_3/Ta_2O_5, MoO_3/Ta_2O_5, WO_3/Ta_2O_5, V_2O_5/Ta_2O_5, and Nb_2O_5/Ta_2O_5. The Raman spectrum of the tantalum oxide support is also shown in Figs. 1–6 and reveals that it is amorphous and possesses the characteristic broad Raman band at ∼ 660 cm^{-1} of $Ta_2O_5 \cdot nH_2O$ [46]. However, the tantalum oxide support will be denoted as Ta_2O_5 in this paper for convenience. At low metal oxide

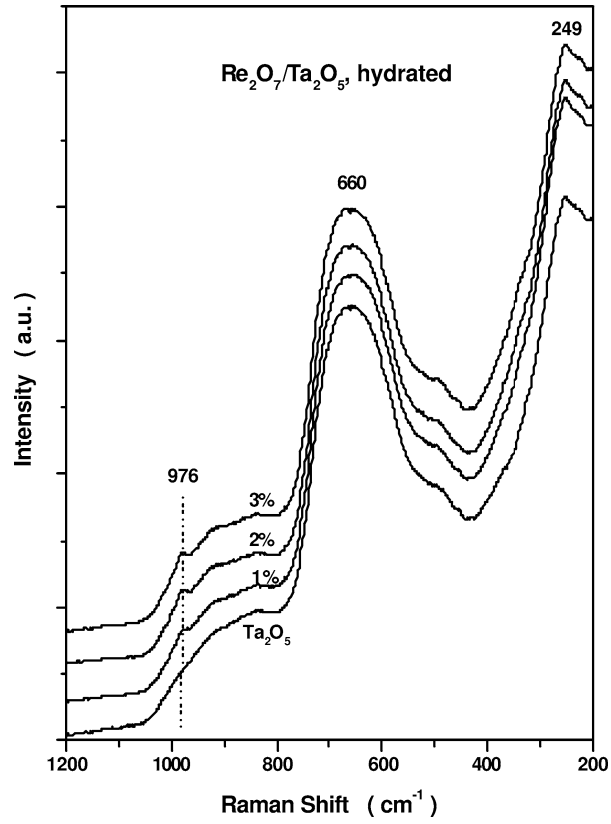

Fig. 1. Raman spectra of Re_2O_7/Ta_2O_5 catalysts under hydrated conditions.

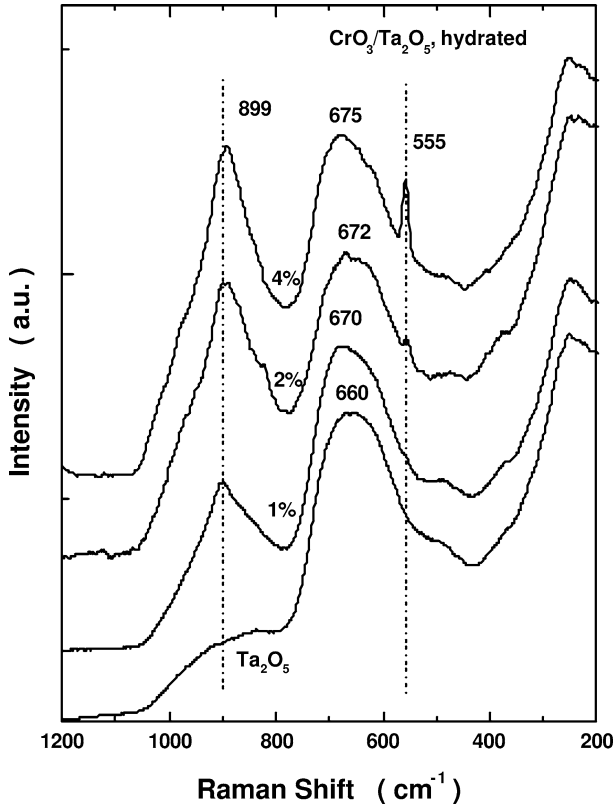

Fig. 2. Raman spectra of CrO_3/Ta_2O_5 catalysts under hydrated conditions.

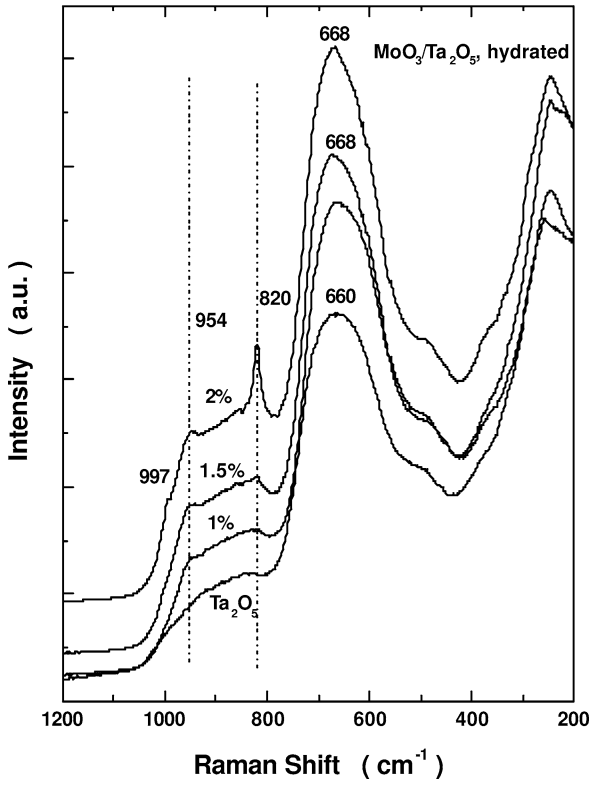

Fig. 3. Raman spectra of MoO_3/Ta_2O_5 catalysts under hydrated conditions.

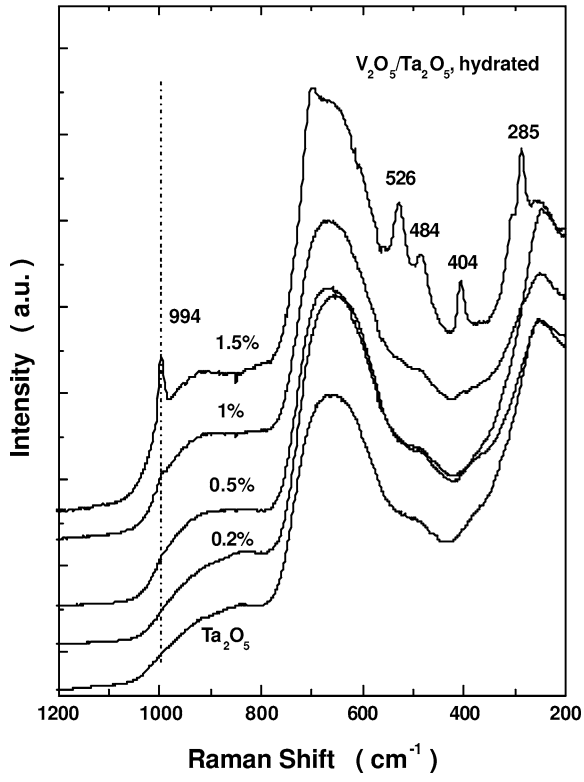

Fig. 5. Raman spectra of V_2O_5/Ta_2O_5 catalysts under hydrated conditions.

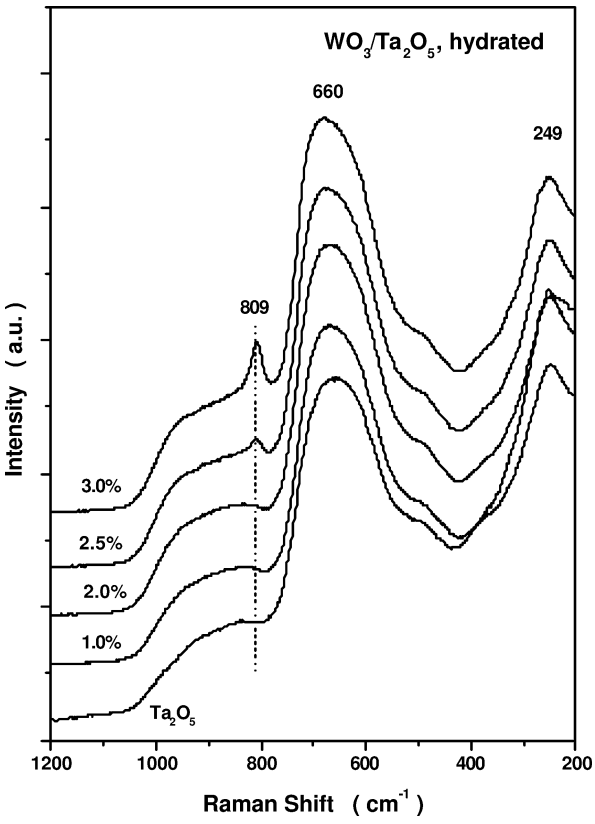

Fig. 4. Raman spectra of WO_3/Ta_2O_5 catalysts under hydrated conditions.

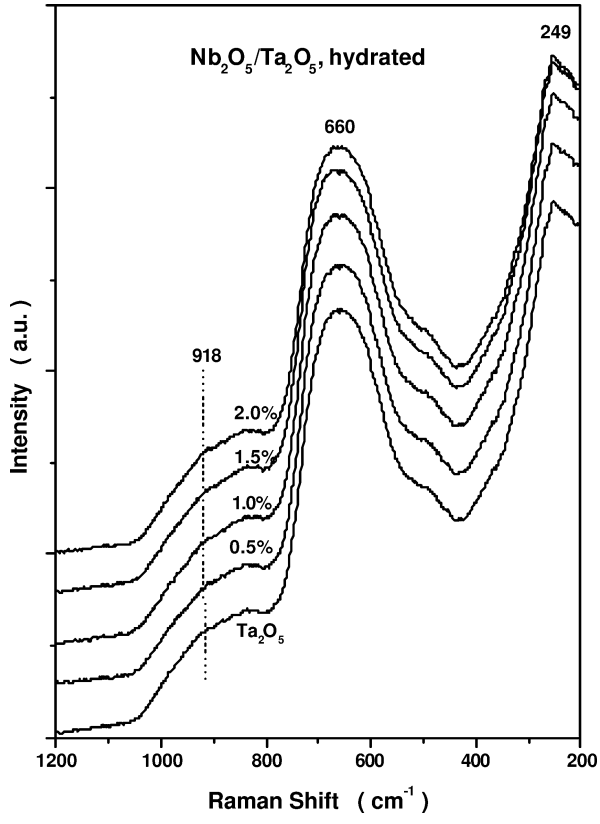

Fig. 6. Raman spectra of Nb_2O_5/Ta_2O_5 catalysts under hydrated conditions.

loadings corresponding to less than monolayer surface coverage, only the Raman signals of the surface metal oxide species are present. Upon increasing the metal oxide loadings above monolayer surface coverage, Raman bands corresponding to the microcrystals of the deposited metal oxides appear and continue to grow: Cr_2O_3 (~ 555 cm^{-1}), MoO_3 (~ 820 cm^{-1} accompanied by a weaker band at ~ 997 cm^{-1}), WO_3 (~ 809 cm^{-1}), and V_2O_5 (~ 994 cm^{-1} as well as many other sharp bands in the 200–600 cm^{-1} region). The metal oxide microcrystals are initially detected for the 2% CrO_3/Ta_2O_5, 1.5% MoO_3/Ta_2O_5, 1.5% V_2O_5/Ta_2O_5, and 2.5% WO_3/Ta_2O_5 catalysts. Monolayer surface coverages of the different supported metal oxides on Ta_2O_5 should not exceed the above values since the microcrystals generally form near and after complete formation of the two-dimensional surface metal oxide monolayer [47]. Furthermore, it should be pointed out that the Raman scattering from the metal oxide microcrystallites is $\sim$ 10–100 times stronger than from the corresponding surface metal oxide species [47]. As a first-order approximation, the intensities of the characteristic microcrystal Raman bands are used to determine the different metal oxide monolayer coverages: 1.6% CrO_3/Ta_2O_5, 1.5% MoO_3/Ta_2O_5, 1.3% V_2O_5/Ta_2O_5, and 2.2% WO_3/Ta_2O_5.

The BET surface areas for the supported metal oxide catalysts were determined to be 15.2 m^2/g (2% CrO_3/Ta_2O_5), 15.0 m^2/g (1.5% MoO_3/Ta_2O_5), 16.5 m^2/g (1.5% V_2O_5/Ta_2O_5), and 16.7 m^2/g (2% WO_3/Ta_2O_5). Using these values as approximations of the surface areas for monolayer coverage of the catalysts, the monolayer surface densities of the different metal oxides were calculated to be 6 Cr/nm^2, 4 Mo/nm^2, 5 V/nm^2, and 4 W/nm^2. The much lower surface areas of the Ta_2O_5 support compared to other metal oxide supports increase the error associated with the monolayer surface coverage determination on the Ta_2O_5 support. Nevertheless, with the exception of surface VO_x on Ta_2O_5, the monolayer surface densities determined for surface metal oxides on Ta_2O_5 are very close to those found on other oxide supports [47].

Monolayer surface coverage for the Re_2O_7/Ta_2O_5 and Nb_2O_5/Ta_2O_5 catalysts could not be determined from Raman spectroscopy. As shown in Figs. 1 and 4, the vibration of the surface ReO_x species is observed at ~ 976 cm^{-1} in Re_2O_7/Ta_2O_5 catalysts, however, crystalline Re_2O_7 is volatile and does not remain on the oxide support after calcination [38]. Furthermore, because of the volatilization of rhenia dimers, monolayer surface coverage is never achieved on any oxide support [38]. No distinct Raman bands for the Nb_2O_5 microcrystals were observed in the Nb_2O_5/Ta_2O_5 catalysts because of the similar vibrations for Nb_2O_5 and Ta_2O_5.

3.1.2. Surface metal oxide species below monolayer surface coverage: hydrated and dehydrated conditions

The Raman spectra of some of the dehydrated tantalum oxide-supported metal oxides were also measured

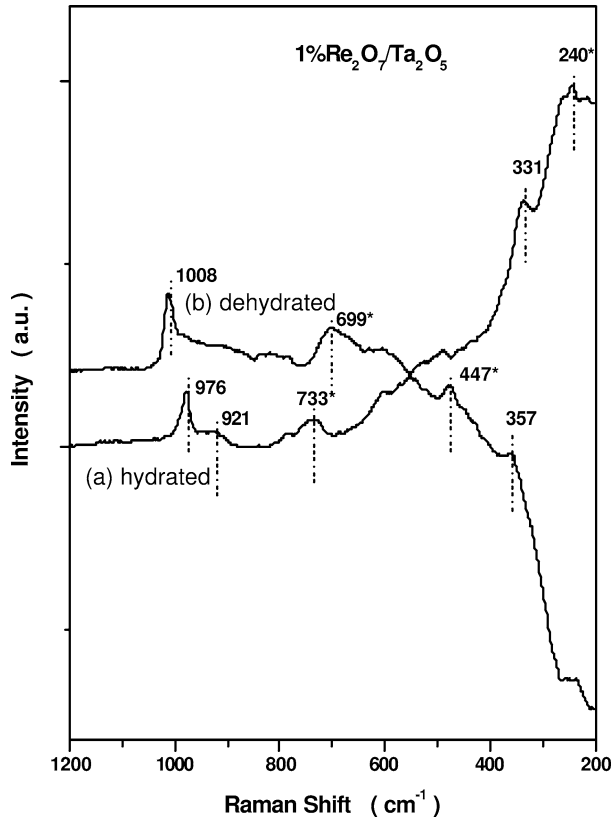

Fig. 7. Raman spectra of 1% Re_2O_7/Ta_2O_5 catalyst under (a) hydrated and (b) dehydrated conditions after subtraction of the spectrum of the Ta_2O_5 support.

(1% CrO_3/Ta_2O_5, 1% MoO_3/Ta_2O_5, 1% Re_2O_7/Ta_2O_5, 1% V_2O_5/Ta_2O_5, and 1% WO_3/Ta_2O_5). However, the Raman signals from the support are very strong relative to those from the surface metal oxide species below monolayer surface coverage. The spectrum of the tantalum oxide support was subtracted from both the hydrated and dehydrated Raman spectra in order to better resolve the Raman bands of the surface metal oxide species. This operation is reasonably effective because the support Raman spectrum consists of a very broad band, and sharper Raman bands from the surface metal oxide species will not be removed by this operation. However, it may also result in some "artificial" bands due to the subtraction of the strong Ta_2O_5 Raman bands. To minimize this shortcoming, three criteria were always employed: (1) the original spectrum was multiplied by a correction factor so that after subtraction the resulting spectrum contained the minimum residual ~ 660 cm^{-1} band of the strong Raman spectrum of the tantalum oxide support, (2) the resultant spectra for the same sample under hydrated and dehydrated conditions should have similar baselines, and (3) before identifying a Raman band of the surface metal oxide species, its comparison with the original Raman spectrum was always necessary.

The background-corrected Raman spectra of 1% Re_2O_7/Ta_2O_5, 1% CrO_3/Ta_2O_5, 1% MoO_3/Ta_2O_5, 1% WO_3/Ta_2O_5, and 1% V_2O_5/Ta_2O_5 under hydrated and dehydrated conditions are presented in Figs. 7–11 and the band positions

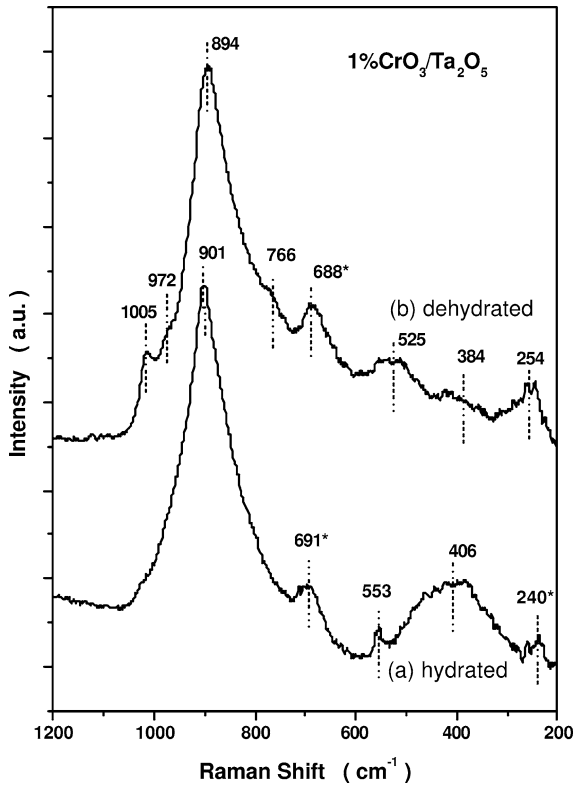

Fig. 8. Raman spectra of 1% CrO_3/Ta_2O_5 catalyst under (a) hydrated and (b) dehydrated conditions after subtraction of the spectrum of the Ta_2O_5 support.

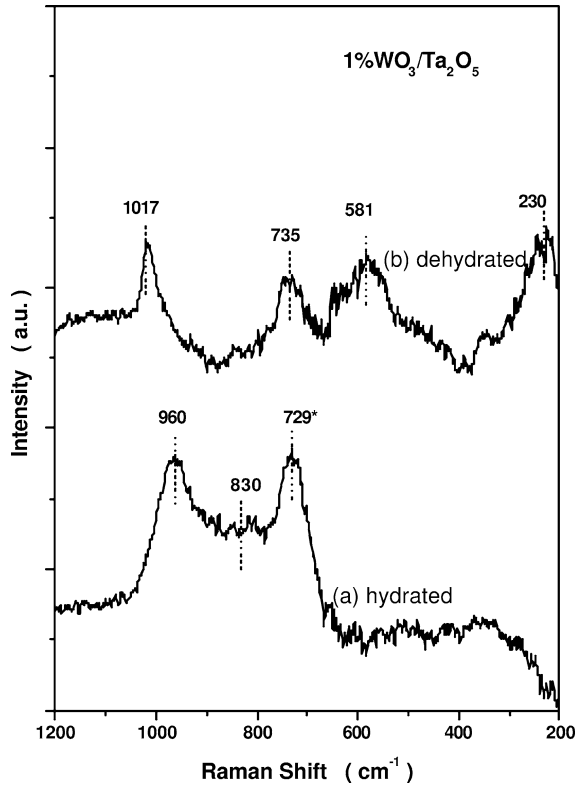

Fig. 10. Raman spectra of 1% WO_3/Ta_2O_5 catalyst under (a) hydrated and (b) dehydrated conditions after subtraction of the spectrum of the Ta_2O_5 support.

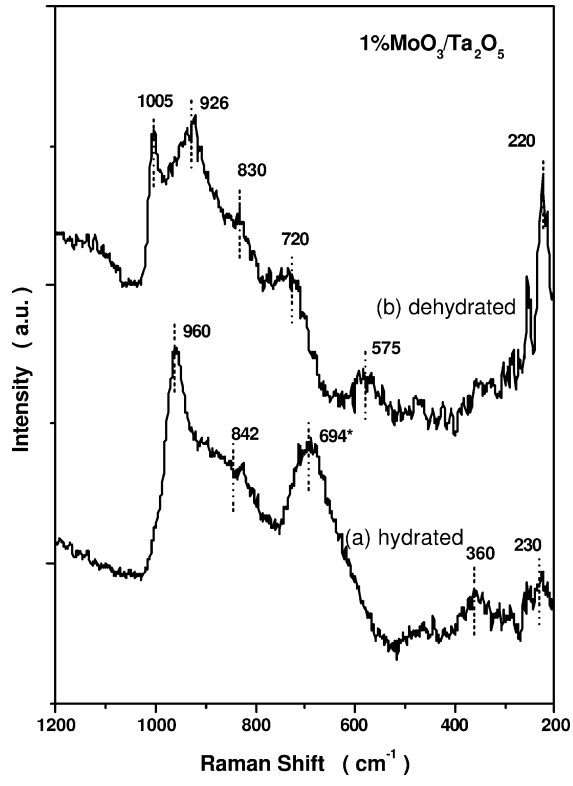

Fig. 9. Raman spectra of 1% MoO_3/Ta_2O_5 catalyst under (a) hydrated and (b) dehydrated conditions after subtraction of the spectrum of the Ta_2O_5 support.

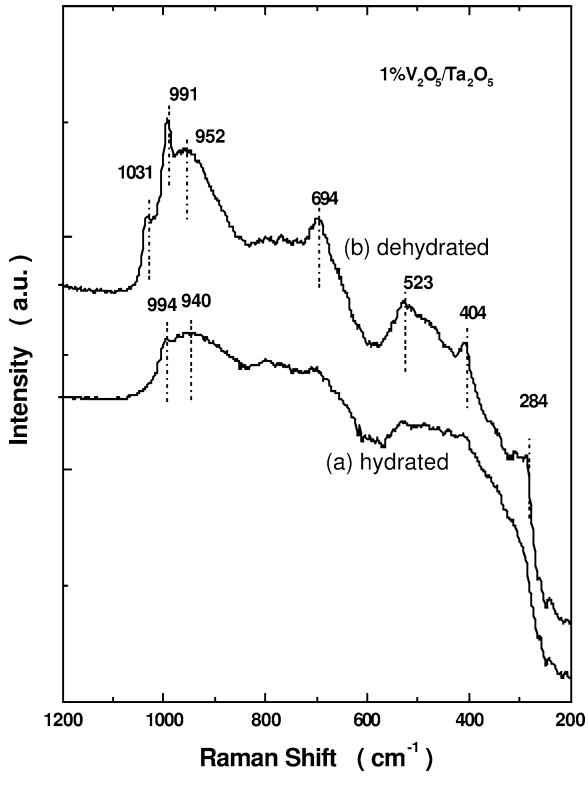

Fig. 11. Raman spectra of 1% V_2O_5/Ta_2O_5 catalyst under (a) hydrated and (b) dehydrated conditions after subtraction of the spectrum of the Ta_2O_5 support.

Table 1
Raman band positions for tantalum oxide-supported metal oxide catalysts under hydrated and dehydrated conditions (cm^{-1})

Catalyst	Hydrated	Dehydrated
1% CrO_3/Ta_2O_5	901, 691,[a] 406, 240[a]	1005, 972, 894, 766,[a] 688,[a] 525,[a] 384, 254
1% MoO_3/Ta_2O_5	960, 842, 694,[a] 360, 230	1005, 926, 830, 720,[a] 575,[a] 220
1% Re_2O_7/Ta_2O_5	976, 921, 733,[a] 331, 240[a]	1008, 699,[a] 447,[a] 357
1% V_2O_5/Ta_2O_5	994, 940	1031, 991, 952, 694,[a] 523,[a] 404, 284
1% WO_3/Ta_2O_5	960, 830, 729[a]	1017, 735,[a] 581,[a] 230

[a] May be "artificial" bands due to background subtraction of the Ta_2O_5 Raman spectrum.

Table 2
Comparison of Raman bands of aqueous metal oxide species with hydrated, ambient surface metal oxide species on Ta_2O_5

Metal oxide species	Aqueous solution (cm^{-1})	On Ta_2O_5 support (cm^{-1})
ReO_4^-	971(s), 916, 332	976, 921, 733,[a] 331, 240[a]
$Cr_2O_7^{2-}$	942, 904(s), 557, 367, 217	901, 691,[a] 406, 240[a]
$Mo_8O_{26}^{4-}$	965(s), 925, 590, 370, 230	960, 842, 694,[a] 360, 230
$HW_{12}O_{42}^{10-}$	955(s), 880, 830, 650, 360, 300	960, 830, 729[a]
$V_{10}O_{28}^{6-}$	994(s), 970, 840, 600, 547, 458, 324, 251, 210, 185	994, 940
$Nb_2O_5 \cdot nH_2O$	880, 630, 280	–

[a] May be "artificial" bands due to background subtraction of the Ta_2O_5 Raman spectrum.

are summarized in Table 1. Due to the characteristics of the Ta_2O_5 background, the Raman bands in the high wavenumber region greater than 800 cm^{-1} are believed to be real, while some of those appearing in the 600–750 cm^{-1} region are most probably "artificial." For example, the Raman bands at $\sim$ 694 cm^{-1} for hydrated 1% MoO_3/Ta_2O_5 and $\sim$ 729 cm^{-1} for hydrated 1% WO_3/Ta_2O_5 catalysts may be the result of a slight difference of the Ta_2O_5 spectrum before and after WO_3 is deposited. The detected Raman bands for the hydrated surface metal oxides on Ta_2O_5 are tabulated in Table 2 and correspond to the Raman bands typically observed for these surface metal oxide species on different oxide supports.

3.2. Methanol oxidation

The methanol oxidation reaction chemically probes the nature of the catalyst surface sites via its reaction products: dimethyl ether results from surface acid sites, CO/CO_2 originate from surface basic sites, and surface redox sites produce formaldehyde, methyl formate, and dimethoxy methane [48]. The pure tantalum oxide support is a solid acid catalyst and the CH_3OH oxidation only yields DME, reflective of surface acidic sites. The catalytic results for methanol oxidation at 230 °C over the different tantalum oxide-supported metal oxide catalysts are presented in Table 3. The 1% WO_3/Ta_2O_5 catalyst exhibits a similar activity as the support for methanol oxidation to DME and Nb_2O_5/Ta_2O_5 is much more active than the support in producing DME during methanol oxidation. The tantalum oxide-supported CrO_3 and V_2O_5 exhibit 100% redox products, while the tantalum oxide-supported MoO_3 and Re_2O_7 reflected the presence of both redox and acidic methanol oxidation reaction products. However, the acidic DME product for the 1% MoO_3/Ta_2O_5 and Re_2O_7/Ta_2O_5 catalysts at least partially originates from the support. Note, that none of the tantalum oxide-supported metal oxide catalysts yield basic CO/CO_2 reaction products at low methanol conversion, which suggests no or little heat and mass transfer limitations because, otherwise, it would result in overoxidation of reaction products to CO/CO_2.

The catalytic activities in Table 3 are expressed as the number of moles of methanol converted per hour per gram of catalyst. The redox TOF values presented in Table 3 are determined by normalizing the redox products by the number of supported metal atoms in the surface metal oxide overlayer. The acidic TOF values are analogously calculated. With the monolayer surface coverage of the different metal oxides on Ta_2O_5 already known from Raman spectroscopy, for a certain loading of a metal oxide below monolayer coverage, the portion of the Ta_2O_5 support surface, which is covered by the metal oxide, can be determined. Thus, the contribution from the acidic Ta_2O_5 support can be deducted from the total activity, and the acidic TOF values of the

Table 3
Selectivities and activities of Ta_2O_5-supported metal oxide catalysts during CH_3OH oxidation at 230 °C

Catalyst	Selectivity (%)				Activity	TOF ($\times 10^{-3}$ s^{-1})	
	HCHO	MF	DMM	DME	($\times 10^{-3}$ mol/(g h))	Redox	Acidic
Ta_2O_5 (L)	0	0	0	100	–	0	17[a]
Ta_2O_5 support	0	0	0	100	1.5	0	–[a]
1% CrO_3/Ta_2O_5	58	42	0	0	10.3	29	0
1% MoO_3/Ta_2O_5	17	25	30	28	11.6	35	10[b]
1% Nb_2O_5/Ta_2O_5	0	0	0	100	8.3	0	31[b]
1% Re_2O_7/Ta_2O_5	0	0	33	67	1.9	5	–
1% V_2O_5/Ta_2O_5	38	38	24	0	29.5	75	0
1% WO_3/Ta_2O_5	0	0	0	100	2.0	0	9[b]

[a] From Ref. [46]. The acidic TOF value for Ta_2O_5 support could be assumed the same as the low temperature phase of crystalline tantalum oxide, Ta_2O_5 (L).
[b] Support activity has been deducted from the total activity.

Ta_2O_5-supported metal oxides can be determined. All of the tantalum oxide-supported metal oxide catalysts are more active than the tantalum oxide support in terms of total activity. In contrast, the acidic TOF values decrease in the order of $NbO_x > TaO_x > MoO_x > WO_x \gg VO_x$. Most of the catalysts exhibiting redox properties produce HCHO, MF, and DMM with the exception of Re_2O_7/Ta_2O_5, which gives only DMM. The redox TOF values decrease in the order of $VO_x \gg MoO_x > CrO_x \gg ReO_x$.

4. Discussion

4.1. Molecular structures of hydrated supported metal oxides on Ta_2O_5

Under hydrated conditions, the aqueous solution chemistry determines the supported oxide molecular structures [31]. According to studies of the hydrolysis of cations [34], the aqueous metal oxide species possess different molecular structures that depend on the aqueous pH and metal oxide concentrations. Isolated ReO_4^- is the only species for rhenium (VII) in aqueous solutions at all pH values. The chromium (VI) species in acidic media forms $HCrO_4^-$ and/or $Cr_2O_7^{2-}$. Under extremely acidic conditions, chromium oxide trimers, $Cr_3O_{10}^{2-}$, and tetramers, $Cr_4O_{13}^{2-}$, are also present in aqueous solutions [49]. For molybdenum (VI), the aqueous cations vary from monomeric MoO_4^{2-} to large clusters, $Mo_{19}O_{59}^{4-}$, with $Mo_7O_{24}^{6-}$, $Mo_8O_{26}^{4-}$, etc. as the solution pH decreases. For tungsten (VI), above a pH of 8–9 only the isolated WO_4^{2-} species is present. As the pH decreases, aqueous $W_6O_{20}(OH)^{5-}$, $W_{12}O_{41}^{10-}$, and $W_{12}O_{39}^{6-}$ are formed. The aqueous chemistry of vanadium (V) is more complicated as the pH decreases, the aqueous species include several isolated monomeric forms (VO_4^{3-}, $VO_3(OH)^{2-}$, $VO_2(OH)_2^-$, $VO(OH)_3$, VO_2^+), linear dimeric $V_2O_7^{4-}$, and metavanadates ($V_3O_9^{3-}$, $V_4O_{12}^{4-}$) and clusters of decavanadates ($V_{10}O_{28-z}(OH)_z^{(6-z)-}$), and the preceding structures increase in concentration as the pH decreases. Aqueous niobium (V) cations form isolated monomers ($Nb(OH)_6^-$, $Nb(OH)_5$, $Nb(OH)_4^+$), and clusters of hexanuclear species ($Nb_6O_{19-z}(OH)_z^{(8-z)-}$).

The highest wavenumber Raman bands were primarily used to identify the hydrated surface metal oxide species on Ta_2O_5 since these bands are strongest and occur in a region where there are no strong Ta_2O_5 Raman vibrations. For the hydrated 1% Re_2O_7/Ta_2O_5, the 976 cm^{-1} band corresponds to the symmetric stretch of aqueous ReO_4^- [20,50]. The hydrated 1% CrO_3/Ta_2O_5 catalyst exhibits the most intense band at $\sim$ 901 cm^{-1}, which excludes the existence of aqueous CrO_4^{2-} and $Cr_4O_{13}^{2-}$ with maxima 846 and 842 cm^{-1}, respectively [51]. The Raman spectra of aqueous $Cr_2O_7^{2-}$ and $Cr_3O_{10}^{2-}$ are very similar; both possess very strong bands at $\sim$ 904 cm^{-1}. The $Cr_3O_{10}^{2-}$ species possesses a medium Raman band at 844 cm^{-1} while the $Cr_2O_7^{2-}$ species does not. Hence, for the hydrated CrO_3/Ta_2O_5 catalysts the chromium (VI) species is consistent with $Cr_2O_7^{2-}$. For aqueous molybdenum (VI) species, previous Raman investigations demonstrated that the maximum Raman band positions for MoO_4^{2-}, $Mo_7O_{24}^{6-}$, and $Mo_8O_{26}^{4-}$ species occur at 897, 943, and 965 cm^{-1}, respectively [36]. The hydrated 1% MoO_3/Ta_2O_5 catalyst possesses a Raman band at 960 cm^{-1}, suggesting the existence of aqueous $Mo_8O_{26}^{4-}$ species. The other Raman bands presented in Table 1 for the hydrated MoO_x species also match the previous results except for the 694 cm^{-1} band, which probably is an artifact from the Ta_2O_5 background subtraction. The characteristic Raman band for the hydrated 1% WO_3/Ta_2O_5 is $\sim$ 960 cm^{-1}, which excludes the existence of aqueous WO_4^{2-} (932 cm^{-1}), $HW_6O_{21}^{5-}$ (962 and 901 cm^{-1}), $H_2W_{12}O_{40}^{6-}$ (978 and 961 cm^{-1}), and $W_{10}O_{32}^{4-}$, according to previous studies [52]. The hydrated surface WO_x species on Ta_2O_5 is most probably para-B-tungstate ($HW_{12}O_{42}^{11-}$) (955 cm^{-1}), which is slightly distorted on the surface. The Raman bands for the hydrated 1% V_2O_5/Ta_2O_5 at 994 and 940 cm^{-1} coincide with the bands for VO_x on Al_2O_3 [31], which suggests that aqueous $V_{10}O_{28}^{6-}$ is the predominate hydrated surface vanadium (V) species. Although there is no significant change of the Ta_2O_5 Raman spectrum when the hydrated surface NbO_x overlayer is present, the surface NbO_x species should form the hydrated $Nb_2O_5 \cdot nH_2O$ clusters because of low pH at PZC of the Ta_2O_5 surface [4].

Comparison of the above results with previous studies of hydrated supported metal oxide systems demonstrates that the molecular structures of the hydrated supported metal oxides on Ta_2O_5 are very similar to the corresponding hydrated metal oxides supported on other oxide supports (e.g., Nb_2O_5, Al_2O_3, TiO_2, and ZrO_2) at low values of pH at PZC. Furthermore, the hydrated molecular structures are consistent with the low pH at PZC values of the Ta_2O_5 support ($\sim$ 2.9) and the active metal oxides Cr_2O_3 ($\sim$ 7.0), MoO_3 ($\sim$ 2.0), WO_3 ($\sim$ 0.4), V_2O_5 ($\sim$ 3.0), and Nb_2O_5 ($\sim$ 2.8) [53].

4.2. Molecular structures of dehydrated surface metal oxides on Ta_2O_5

Upon dehydration, the thin aqueous film present on the support desorbs, and the surface metal oxide species react with the surface Ta–OH groups and form new dehydrated surface metal oxide molecular structures. Under dehydrated conditions, the highest wavenumber Raman bands for the surface metal oxide species shift to higher values. The terminal M=O bonds usually exhibit a symmetric stretching band at $\sim$ 980–1040 cm^{-1}; symmetric stretch of polymeric bridging O–M–O or antisymmetric stretch of bridging M–O–M bonds occur between 600 and 950 cm^{-1}; symmetric stretch of bridging M–O–M at 400–600 cm^{-1}; bending mode of M–O bonds occur at 300–400 cm^{-1}; and bending mode of bridging M–O–M bonds at 200–300 cm^{-1}. Under dehy-

drated conditions, as shown in Figs. 7–11 and Table 1, all the surface metal oxide species are polymerized to some extent because they exhibit both antisymmetric and symmetric stretching modes of polymeric bridging M–O–M or O–M–O bonds.

Comparison of the present investigation of the Ta_2O_5-supported metal oxides with previous detailed studies of other supported metal oxide systems allows for the molecular structural determination of the dehydrated surface MO_x species on Ta_2O_5 [27,54]. The dehydrated surface ReO_x species on the Ta_2O_5 support exhibits a Raman band at 1008 cm^{-1} due to the symmetric stretching mode of the terminal Re=O bond and may be polymerized [54]. For the dehydrated 1% CrO_3/Ta_2O_5, there is a highly distorted polymeric surface CrO_4 species with Raman bands at 1005 and 894 cm^{-1}, which have been assigned to the symmetric stretching modes of terminal Cr=O and bridging O–Cr–O bonds, respectively [55]. For the dehydrated 1% MoO_3/Ta_2O_5, the major surface MoO_x species also possesses a highly distorted polymeric surface MoO_6 structure, the Raman bands at 1005 and 926 cm^{-1} have been assigned to the symmetric stretching modes of the terminal Mo=O and the polymeric bridging O–Mo–O bonds, respectively [36]. Similarly, for the dehydrated 1% WO_3/Ta_2O_5, the major surface WO_x species is a highly distorted polymeric surface WO_6 structure, and the Raman band at 1017 cm^{-1} is assigned to the symmetric stretching mode of the terminal W=O bond. The dehydrated surface VO_x species on the Ta_2O_5 support possesses both highly distorted isolated and polymeric VO_4 structures with Raman bands at 1031 and 952 cm^{-1} for the symmetric stretching modes of the terminal V=O and bridging O–V–O bonds. There are no detectable Raman bands for the dehydrated surface NbO_x species on Ta_2O_5 for 1% Nb_2O_5/Ta_2O_5 because of the weak surface NbO_x Raman bands relative to the stronger Raman bands for the Ta_2O_5 support. However, the predominant dehydrated surface NbO_x species on Ta_2O_5 is expected to be the highly distorted polymeric NbO_5/NbO_6 structures [40]. Previous Raman and IR studies revealed that surface NbO_x species only possess one terminal Nb=O bond and are primarily polymerized [56].

Comparison of the above results with previous studies of various supported metal oxide species reveals that the dehydrated molecular structures of the surface metal oxides on Ta_2O_5 support are very similar to the corresponding surface metal oxide species on other oxide supports, (e.g., Nb_2O_5, Al_2O_3, TiO_2, and ZrO_2). Furthermore, the dehydrated surface metal oxides on Ta_2O_5 appear to favor a higher concentration of polymerized surface species (e.g., there are no isolated species detected at $\sim$ 1030 cm^{-1} for CrO_3/Ta_2O_5).

4.3. Molecular structure–activity/selectivity relationships

For the methanol oxidation reaction, the Ta_2O_5-supported metal oxides are more active than the pure Ta_2O_5 support and most of the catalysts possess redox properties that the Ta_2O_5 support does not. For the redox catalysts, the supported vanadia catalyst is most active, and the TOF (redox) values vary as follows: $V_2O_5 > MoO_3 \sim CrO_3 > Re_2O_7 \gg WO_3$ (see Table 3).

Table 4
Redox TOFs of metal oxides supported on tantalum oxide and niobium oxide during CH_3OH oxidation at 230 °C

Metal oxide	Redox TOF ($\times 10^{-3}$ s^{-1})	
	Ta_2O_5 support	Nb_2O_5 support
Re_2O_7	5	15
CrO_3	29	46
MoO_3	35	15
WO_3	0	0
V_2O_5	75	85

Compared to the corresponding Nb_2O_5-supported metal oxide catalysts [50], which have similar dehydrated molecular structures as the corresponding Ta_2O_5-supported metal oxide catalysts, the Ta_2O_5-supported metal oxide catalysts exhibit comparable TOF (redox) or at least within a factor of 3 (see Table 4). The somewhat lower electronegativity of Ta(V) than Nb(V) would have been expected to result in a slightly higher TOF (redox) for the Ta_2O_5-supported metal oxide catalysts [26]. However, this difference may not have been significant enough within the experimental error of the TOF (redox) calculations. The TOF (acidic) could not be quantitatively compared because the high surface area of Nb_2O_5 and the low surface coverage of the metal oxides, $\theta \leqslant 20\%$, resulted in a significant acidic contribution from the support [50].

There does not appear to be a relationship between the TOF (redox) and the molecular structures of the dehydrated surface metal oxides present under reaction conditions [47]. Surface VO_x and CrO_x species both consist of MO_4 units, but the TOF (redox) for V_2O_5/Ta_2O_5 is much greater than for CrO_3/Ta_2O_5. Similarly, surface MoO_x and WO_x species both consist of MO_5/MO_6 units, but surface MoO_x predominantly forms redox products and surface WO_x exclusively yields acidic products (DME). Thus, the relative redox activity depends on the specific nature of the metal oxide being employed since for the pure metal oxides the methanol oxidation TOF (redox) follows the exact same trend: $V_2O_5 > MoO_3 \gg WO_3$ [57].

Another interesting observation is that the more active surface redox sites generally yielded higher selectivity to redox products: $V_2O_5 \sim CrO_3 > MoO_3 > Re_2O_7$. This suggests that generally the more active the surface redox sites relative to the exposed surface acidic sites of the Ta_2O_5 support, the higher the selectivity to redox products. In addition, the intrinsic redox/acidic character of the specific surface metal oxide will also significantly influence the selectivity of the surface metal oxide species.

5. Conclusions

The metal oxides Re_2O_7, CrO_3, MoO_3, WO_3, V_2O_5, and Nb_2O_5 form two-dimensional overlayers on the tantalum oxide support. The hydrated molecular structures of these surface metal oxides under ambient conditions correspond to ReO_4^-, $Cr_2O_7^{2-}$, $Mo_8O_{26}^{4-}$, $HW_{12}O_{42}^{11-}$, $V_{10}O_{28}^{6-}$, and $Nb_2O_5 \cdot nH_2O$ species present in acidic aqueous solutions. Upon dehydration, only one dehydrated surface ReO_4 species is present on tantalum oxide support. For CrO_3, MoO_3, WO_3, V_2O_5, and Nb_2O_5 supported on tantalum oxide, two dehydrated surface metal oxide species can be present: isolated and/or polymerized surface metal oxide species. The surface vanadium, molybdenum, chromium, and rhenium oxide sites on tantalum oxide behave as surface redox sites, and the surface tungsten and niobium oxide sites on tantalum oxide are surface acidic sites as probed by methanol oxidation. The surface molybdenum oxide sites on tantalum oxide possess both surface acid and redox characteristics. The TOF (redox) for the Ta_2O_5-supported metal oxide catalysts are comparable to the corresponding Nb_2O_5-supported metal oxide catalysts because of the rather similar electronic and chemical properties of Nb_2O_5 and Ta_2O_5. The redox activity and selectivity of the various surface metal oxides on Ta_2O_5 reflect the natural redox properties of these pure metal oxides and the more active surface redox sites minimized the contribution from the surface acidic sites of the Ta_2O_5 support.

Acknowledgment

The financial support of H.C. Starck for this research is gratefully acknowledged.

References

[1] C.L. Thomas, Catalytic Processes and Proven Catalysts, Academic Press, New York, 1970.
[2] J. Pasel, P. Kassner, B. Montanari, M. Gazzano, A. Vaccari, W. Makowski, T. Lojewski, R. Dziembaj, H. Papp, Appl. Catal. B: Environ. 18 (1998) 199.
[3] G. Deo, I.E. Wachs, J. Catal. 146 (1994) 323.
[4] J.-M. Jehng, I.E. Wachs, Catal. Today 8 (1990) 37.
[5] S.D. Yim, K.-H. Chang, D.J. Koh, I.-S. Nam, Y.G. Kim, Catal. Today 63 (2000) 215.
[6] H. Yang, L. Lin, Q. Wang, L. Xu, S. Xie, S. Liu, Stud. Surf. Sci. Catal. 136 (2001) 87.
[7] S. Wang, K. Murata, T. Hayakawa, S. Hamakawa, K. Suzuki, Appl. Catal. A: Gen. 196 (2000) 1.
[8] B.M. Weckhuysen, R.A. Schoonheydt, Catal. Today 51 (1999) 215.
[9] D.S. Kim, I.E. Wachs, K. Segawa, J. Catal. 146 (1994) 268.
[10] T.J. Yang, J.H. Lunsford, J. Catal. 103 (1987) 55.
[11] D. Wang, J.H. Lunsford, M.P. Rosyneck, Top. Catal. 3 (1996) 289.
[12] S. Li, C.-L. Zhang, Q.-B. Kan, J.-F. Yu, Y. Yuan, T.-H. Wu, Stud. Surf. Sci. Catal. 130 (2000) 3609.
[13] F. Solymosi, J. Cserenyi, A. Szoke, T. Bansagi, A. Oszko, J. Catal. 165 (1997) 150.
[14] Y.C. Park, H.K. Phee, Appl. Catal. A: Gen. 179 (1999) 145.
[15] J.C. Yori, C.R. Vera, J.M. Parera, Appl. Catal. A: Gen. 163 (1997) 165.
[16] E. Iglesia, D.G. Barton, S.L. Soled, S. Miseo, J.E. Baumgartner, W.E. Gates, G.A. Fuentes, G.D. Meitzner, Stud. Surf. Sci. Catal. 101 (1996) 533.
[17] L.L. Murrell, C.J. Kim, D.C. Grenoble, US patent 4,233,139, 1980.
[18] Special issue on olefin metathesis, J. Mol. Catal. 76 (1992).
[19] Y. Yuan, Y. Iwasawa, J. Phys. Chem. 106 (2002) 4441.
[20] D.S. Kim, I.E. Wachs, J. Catal. 141 (1993) 419.
[21] M. Schmal, V. Teixeira da Silva, F.B. Noronha (Eds.), Catal. Today 57 (2000), special issue devoted to group five compounds.
[22] K. Tanabe (Ed.), Catal. Today 28 (1996), special issue devoted to niobium oxide compounds.
[23] K. Tanabe (Ed.), Catal. Today 16 (1993), special issue devoted to niobium oxide compounds.
[24] E. Ko (Ed.), Catal. Today 8 (1990), special issue devoted to niobium oxide compounds.
[25] M.D. Argyle, K. Chen, A.T. Bell, E. Iglesia, J. Catal. 208 (2002) 139.
[26] I.E. Wachs, J. Catal. 13 (1998) 37.
[27] I.E. Wachs, Catal. Today 27 (1996) 437.
[28] M.A. Vuurman, F.D. Hardcastle, I.E. Wachs, J. Mol. Catal. 84 (1993) 193.
[29] D.S. Kim, K. Segawa, T. Soeya, I.E. Wachs, J. Catal. 136 (1992) 539.
[30] J.-M. Jehng, I.E. Wachs, J. Mol. Catal. 67 (1991) 369.
[31] G. Deo, I.E. Wachs, J. Phys. Chem. 95 (1991) 5889.
[32] M.A. Vuurman, D.J. Stufkens, A. Oskam, I.E. Wachs, J. Mol. Catal. 76 (1992) 263.
[33] S.D. Kohler, J.G. Ekerdt, D.S. Kim, I.E. Wachs, Catal. Lett. 16 (1992) 231.
[34] C.F. Baes, R.E. Mesmer Jr., The Hydrolysis of Cations, Wiley, New York, 1976.
[35] H. Eckert, I.E. Wachs, J. Phys. Chem. 93 (1989) 6796.
[36] H. Hu, I.E. Wachs, S.R. Bare, J. Phys. Chem. 99 (1995) 10897.
[37] B.M. Weckhuysen, L.M. De Ridder, R.A. Schoonheydt, J. Phys. Chem. 97 (1993) 4756.
[38] F.D. Hardcastle, I.E. Wachs, J.A. Horsley, G.H. Via, J. Mol. Catal. 46 (1988) 15.
[39] J.A. Horsley, I.E. Wachs, J.M. Brown, G.H. Via, F.D. Hardcastle, J. Phys. Chem. 91 (1987) 4014.
[40] T. Tanaka, T. Yoshida, H. Yoshida, H. Aritani, T. Funabiki, S. Yoshida, J.-M. Jehng, I.E. Wachs, Catal. Today 28 (1996) 71.
[41] T. Ushikubo, K. Wada, J. Catal. 148 (1994) 138.
[42] T. Tanaka, H. Nojima, T. Yamamoto, S. Takenaka, T. Funabiki, S. Yoshida, Phys. Chem. Chem. Phys. 1 (1999) 5235.
[43] H. Noureddini, M. Kanabur, J. Assoc. Off. Anal. Chem. 76 (1999) 305.
[44] I.E. Wachs, US patent 4,544,649, 1985.
[45] M. Baltes, A. Kytökivi, B.M. Weckhuysen, R.A. Schoonheydt, P.V.D. Voort, E.F. Vansant, J. Phys. Chem. B 105 (2001) 6211.
[46] Y. Chen, J.L.G. Fierro, T. Tanaka, I.E. Wachs, J. Phys. Chem. B, in press.
[47] M.A. Bañares, I.E. Wachs, J. Raman Spectrosc. 33 (2002) 359.
[48] J.M. Tatibouët, Appl. Catal. A: Gen. 148 (1997) 213.
[49] G. Michel, R. Cahay, J. Raman Spectrosc. 17 (1986) 4.
[50] J.-M. Jehng, A.M. Turek, I.E. Wachs, Appl. Catal. A: Gen. 83 (1992) 179.
[51] F.D. Hardcastle, I.E. Wachs, J. Mol. Catal. 46 (1988) 173.
[52] M.M. Ostromecki, L.J. Burcham, I.E. Wachs, N. Ramani, J.G. Ekerdt, J. Mol. Catal. A: Chem. 132 (1998) 43.
[53] M. Kosmulski, Chemical Properties of Material Surfaces, Dekker, New York, 2001.
[54] B.M. Weckhuysen, J.-M. Jehng, I.E. Wachs, J. Phys. Chem. B 104 (31) (2000) 7382.
[55] D.S. Kim, I.E. Wachs, J. Catal. 142 (1993) 166.
[56] L.J. Burcham, J. Datka, I.E. Wachs, J. Phys. Chem. B 103 (29) (1999) 6015.
[57] M. Badlani, I.E. Wachs, Catal. Lett. 75 (2001) 137.